Austin Journal of Biotechnology & Bioengineering

Open Access

Austin Publishing Group

Research Article

Effects of Ag/SiO_2 Nanoparticles on Gene Expression of Digestive α-Amylase in Colorado Potato Beetle

Ashouri S[1], Dolatyari M[2], Pourabad RF[1], Rostami A[2,3]* and Mirtaghioglu H[4]

[1]Department of Plant Protection, Faculty of Agriculture, University of Tabriz, Tabriz, Iran

[2]SP-EPT Labs, ASEPE Company, Industrial Park of Advanced Technologies, Tabriz, Iran

[3]OIC Research Group, University of Tabriz, Tabriz, Iran

[4]Faculty of Science and Literature, Department of Statistics, University of Bitlis Eren, Bitlis, Turkey

***Corresponding author:** Ali Rostami, SP-EPT Labs, ASEPE Company, Industrial Park of Advanced Technologies, Tabriz, Iran; OIC Research Group, University of Tabriz, Tabriz-5166614761, Iran

Received: March 31, 2022; **Accepted:** April 26, 2022; **Published:** May 03, 2022

Abstract

Insecticidal properties of nanoparticles (NPs) have been considered widely in different studies. In this study, synthesis of Ag/SiO_2 NPs is reported and the effect of the nanoparticles on the digestive α-amylase gene expression in the Colorado potato beetle (CPB), *Lepidoptera decemlineata* say is investigated. For this purpose, the inhibition of fourth instar larval digestive α-amylase with NPs was analyzed by different concentrations, and the highest inhibitory effect was recorded (72%) at 1000 ppm of Ag/SiO_2 NPs. Mortality for the reared larvae from the first instar on potato leaves coated with 1000 ppm Ag/SiO_2 NPs was 65%, while it is 8% for the control trial. To investigate the process, we conjugated the nanoparticles with extracted RNA, and the photoluminescent (PL) spectra of the obtained materials were measured and investigated. The results indicate that the FRET phenomenon occurs when the RNA reacts with nanoparticles. These results are according to the PL spectra of RNAs extracted from the larval fed with nanoparticles. The structure is simulated and calculated by the DFT method. The obtained results confirm chemical interaction between nanoparticles and nitrogenous bases on the RNA which can decrease gene expression (0.47 fold) compared to control and causes inhibition of larvae's growth.

Keywords: α-amylase; Ag/SiO_2; Nanoparticles; Gene expression; RT-qPCR; FRET; DFT

Introduction

Indiscriminate use of pesticides causes some adverse effects on the environment such as increased pest resistance, reduced soil biodiversity, reduced nitrogen fixation, and decreased pollinators [1]. Hence, it is necessary to introduce new innovative technologies and methods to overcome these problems [2]. Biocompatible, biodegradable, and intelligent materials are currently an emerging area of interest in the field of efficient and safe pesticide formulation [3]. The nanoscale sciences have great importance in the agricultural revolution and one of the key focus areas for nanotechnology agricultural research is nano pesticides [1]. Therefore, there is a need to investigate the effects of nanoparticles (NPs) on insect pest species. The employment of NPs obtained through various synthesis routes as novel pesticides have recently attracted high research attention [4]. A notable number of researches have been conducted to test their toxic potential against a wide number of insect pests and vectors; ZnO NPs causes mortality and reduction in wood-feeding of *Reticulitermes flavipes* (Kollar) (Isoptera: Rhinotermitidae) [5] and shows insecticidal activity on adults of *Trialeurodes vaporariorum* (Westwood) (Hemiptera: Aleyrodidae) [6]; SiO_2 NPs causes midgut epithelial injury in intoxicated workers of *Bombus terrestris* (L.) (Hymenoptera: Apidae) [7]; Ag NPs has acute and chronic toxic effects on *Drosophila melanogaster* (Meigen) (Diptera: Drosophilidae) [8] and induces midgut epithelial cell damage in *Aedes aegypti* (L.) (Diptera: Culicidae) [9]. Amylase, protease, lipase, and invertase activities of *Spodoptera litura* (Fabricius) (Lepidoptera: Noctuidae) decrease when exposed to Ag NPs [10]. Also, Ag Nps induces oxidative stress in the larvae of *S. litura* and *Achaea Janata* (L.) (Lepidoptera: Erebidae), which is countered by antioxidant enzymes [11]. Ingestion of Ag NPs in D. melanogaster during the adult stage for a short and long time significantly affects egg-laying capability along with impaired ovarian growth [12]. As recently pointed out, total protein levels, acetylcholinesterase, α, and β carboxylesterase activities decrease in *Aedes albopictus* (Skuse) and *Culex pipiens* (L.) (Diptera: Culicidae) when exposes to Ag NPs [13]. In addition, Ag NPs induce a decrease in total proteins, esterase, and phosphatase enzymes in the fourth instar larvae of *A. albapictus* [14]. Studies on the insecticidal effects of chemical or biological insecticides and their nanoparticles have been conducted as the effects of imidacloprid and Ag-Zn NPs on *Aphis nerii* (Fonscolombe) (Hemiptera: Aphididae) [15], and the entomopathogenic bacterium, *Bacillus thuringiensis* kurstaki (Btk) synthesized Ag NPs on *Trichoplusia ni* (Hubner) [16]. It has been found out greater insecticidal effects for NPs. Larvicidal activity of the bio-synthesized Au NPs using *Artemisia vulgaris* (L.) leaf extract has been found against *A. aegypti* and shows that Au NPs cause damage to the midgut, epithelial cells, and cortex [17].

It is well known that due to their similar size to cellular proteins, NPs can cross some of the barriers of biological systems. Toxicity mechanisms of NPs include disruption of membranes, oxidation of proteins, interruption of energy transduction, the formation of reactive oxygen species, the release of toxic constituents, and genotoxicity [18]. Concerning the genotoxic activity of NPs; Ag NPs has genotoxicity in the fourth instar larvae of *Chironomus riparius* (Meigen) (Diptera: Chironomidae) [19]. Glutathione-S-transferase genes up-or down-regulated in *C. riparius* according to the tested concentration of Ag NPs and Cd NPs [20], also Ag NPs

Citation: Ashouri S, Dolatyari M, Pourabad RF, Rostami A and Mirtaghioglu H. Effects of Ag/SiO_2 Nanoparticles on Gene Expression of Digestive α-Amylase in Colorado Potato Beetle. Austin J Biotechnol Bioeng. 2022; 9(1): 1116.

led to prominent induction of genes related to oxidative stress and detoxification in *C. riparius* [21]. Genotoxic activities of Ag NPs, Co NPs, and Ni NPs have been demonstrated on *D. melanogaster* [22-25]. The genotoxic effects of Ag NPs biosynthesized using neem cake against larvae and pupae of A. aegypti have been evaluated [26]. *Bombyx mori* (L.) (Lepidoptera: Bombycidae) some cells signaling pathway genes were up-regulated by TiO_2 NPs [27]. However, physiological events within the cell caused by the NPs are a question about the genotoxic effects of NPs [18]. Metal nanoparticles can bind to sulfur from proteins or to phosphorus from nucleic acids which lead to rapid denaturation of organelles and enzymes [4]. There is no report on the genotoxic effect of NPs on CPB, especially on digestive α-amylase enzyme gene expression. Therefore in the current investigation, a qPCR-based assay for amylase expression in the fourth instar larvae of *L. decemlineata* in response to Ag/SiO_2 nanoparticles was developed. Moreover, to further understand the mechanism of action, the interaction between the insect's RNA and nanoparticles was screened using the fluorescence resonance energy transfer (FRET) technique. Fluorescence resonance energy transfer (FRET) is a nonradiative energy transfer process in which energy transfers from an excited state of a donor to an energy level in the structure of the acceptor through long-range dipole-dipole interactions [28-33]. In this way, the acceptor absorbs the energy of the donor at the emission wavelengths. The acceptor does not need to remit the energy using the fluorescent process. The rate of energy transfer depends on the content of spectral overlap, the transition dipoles orientations, and the gap between the donor and acceptor [28-40].

Materials and Methods

Materials required for synthesis Ag/SiO_2 nanoparticles

Materials used and their suppliers are as follows: $AgNO_3$ (99% Sigma-Aldrich), polyvinyl pyrrolidone (PPV) K17 (M. W. 8000) (99% Sigma-Aldrich), tetraethyl orthosilicate (TEOS, Sigma), 30% NH4OH (25% Merck), ethanol (96% Merck).

Synthesis of Ag nanoparticles

Ag nanoparticles were fabricated by reducing Ag ions from the $AgNO_3$ solution with $NaBH_4$ solution. Briefly, 20mL of $AgNO_3$ (0.1M) was added to the 3% solution of polyvinyl pyrrolidone (PPV) and stirred for 15min. 40mL of the $AgNO_3$ (0.1M) was added dropwise to the solution. The solution was allowed to age at room temperature, in the dark, for 1h. The nanoparticles were centrifuged three times, 30min each time with water and ethanol.

Synthesis of nanoparticles coated with silica

The Ag nanoparticles were coated with silica with the following procedure. 7mL of a concentrated Ag nanoparticle solution was mixed with 40mL of ethanol and 400µL of 30% NH_4OH, and subsequently, 4µg of TEOS was quickly added. The reaction was allowed to proceed for 45min at room temperature under vigorous stirring and then was stored in the refrigerator at 4°C for 24h then the synthesized Ag/SiO_2 nanoparticles were centrifuged and re-suspended in 10mL of deionized water.

Conjugation of the RNA with the synthesized Ag/SiO_2 NPs

Two mL of the synthesized nanoparticles with the concentration of 30 ppm were added on 10mL of the diluted RNA (30 ppm) and the mixture was stirred for 1h. The temperature was 0°C. The obtained solution was centrifuged and washed several times by water and redispersed in 10mL of water.

DFT calculations

The electronic band structure along with the density of states (DOS) of bare Ag/SiO_2 QD and its conjugation with Cytosine were calculated using DFT. Calculations were done with the CASTEP code [41] and optimized using the BFGS (Broyden-Fletcher-Goldfarb-Shanno) geometry optimization method [41]. In the calculation, Generalized gradient approximation (GGA) and the non-local gradient-corrected exchange-correlation functional as parameterized by Perdew-Burke-Ernzerhof (PBE) used which applies a plane wave basis set for the valence electrons and norm-conserving pseudopotential (NCP) [42] for the core electrons. The number of plane waves included in the basis was determined from cut-off energy (Ec) of 500.0eV. The summation over the Brillouin zone was carried out with k point sampling using a Monkhorst-Pack grid [43]. Geometry optimization under applied hydrostatic pressure with parameters of 3×3×3 was used to determine the modulus of a material (B) and its pressure derivative, B' = dB/dP [44].

Insect rearing

The colony of CPB was collected from Ajabshir province of East Azarbayjan, Iran; maintained on potato foliage cultivar Agria, which tubers were supplied from Potato Research Center of Ardabil, Ardabil, Iran, and planted at the University of Tabriz, Tabriz, Iran. The rearing condition was about 27 ± 1 °C, 60 ± 5% relative humidity, 16:8 h (L:D) photoperiod, and white fluorescent light. Insects were reared from egg hatch to adult in clear plastic dishes containing daily fresh potato leaves.

Preparation of enzyme source for activity assays

Ten guts from fourth instar larvae (L4) of CPB were isolated by dissection and homogenized in 500µL cold distilled water. The mixture was centrifuged at 10000 rpm for 30min at 4°C. The supernatant was stored as an enzyme source at -20°C before analysis. The protein concentration of the enzyme samples was adjusted to 3mg/ml.

Amylase inhibition assay

The Alpha-amylase activity was measured by the dinitrosalicylic acid (DNS) procedure [45], using a 1% soluble starch as previously described [46]. In the laboratory inhibition assays, the enzyme extract was pre-incubated with 10µL Ag/SiO_2 NPs at different concentrations (125, 250, 500, 1000, 2000, and 4000 ppm) before the addition of substrate for 30min at 37°C. The percentage of inhibition was calculated compared to control.

Feeding trials

Twenty-five newly emerged CPB larvae were reared on excised "Agria" potato leaves which were placed in aerated plastic arenas. The leaves were painted with 1000 ppm Ag/SiO_2 NPs and replaced daily throughout the experiment. In control, insects fed with potato leaves were painted with xH_2O. After ten days, the mortality of larvae (up to reaching L4 instar) was recorded and survived L4s were used in RNA extraction.

Total RNA isolation

Total RNA was isolated from three individuals of L4 whole body which were crushed in liquid nitrogen, and with the addition of the

RNX-PLUS Solution (EX6101, Cinnagen®, Tehran, Iran) according to the manufacturer's instruction with some modifications as follows: 1mLice cold solution was immediately added to the homogenized sample and incubated at room temperature for 5min. Samples were centrifuged at 12000 rpm at 4°C for 15min for removing non-homogenized particles. Then, 300µL chloroform was added and after vigorous shaking incubated on ice for 15min. Samples were centrifuged at the same condition and RNA was precipitated by adding the same volume of isopropanol to the upper phase and incubated on ice for 15min. After centrifugation, the pellet containing RNA was dislodged with 1mL of 75% ethanol and then centrifuged. This washing process was repeated twice to remove all chemical contamination. The pellet was left to dry at room temperature for a few minutes and dissolved in 50µL DEPC treated water. The purified RNAs were immediately used in the cDNA synthesis or were stored at -80°C until subsequent analysis.

The total RNA concentration was determined with appropriate dilution (1:100) using a photometer (Eppendorf®, Hamburg, Germany) at wavelengths from 260 and 280 nm where only total RNAs with A260/280 ratio ranging between 1.8-2 were used for further application.

The integrity of RNA was verified in 1% agarose (Sigma®, St Louis, MO, USA) gel electrophoresis stained with ethidium bromide by using loading dye containing formamide which allows RNA fragments to be separated. RNA samples were heat-denatured before separation at 70°C for 5min. The agarose gels were visualized under ultraviolet light.

Reveres transcription-PCR (RT-PCR)

Synthesize of cDNA (179bp) from high integrity and purify total RNA was performed using cDNA synthesis kit (YT4500, YTA®, Tehran, Iran) with oligo (dT)18 primer and M-MLV reverse transcriptase, following the protocol recommended by the manufacturer, as follow; 2µL total RNA (1µg/mL) was combined with 1µL oligo (dT)18 primer (50µM) and DEPC treated water to a final volume of 13.4µL. RNA and primers were denatured at 7°C for 5min using Primus 25 advanced thermocycler (PEQLAB Biotechnologie GmbH, Erlangen, Germany) and then incubated on ice for 5min. cDNA synthesis mix contained 4µL first strand buffer, 1µL dNTP (10mM each), 0.5µL RNasin (40U/µL) and 1µL M-MLV reverse transcriptase was added and incubation was continued at 42°C for 60min. The reaction was terminated by heating at 70°C for 5min. The synthesized cDNAs were stored at -20°C until analysis.

The RT-PCR products were subjected to gradient PCR (48-58°C) using Taq DNA Polymerase 2x Master Mix Red (Ampliqon®, Bie & Berntsen, Herlev, Denmark) at 94°C for 5min, followed by 35 cycles of denaturing at 94°C for 60sec, annealing at gradient temperatures for 40sec, extending at 72°C for 60sec and a final elongation step at 72°C for 7min. After optimizing annealing temperature, the PCR was carried out at 50°C. Also, the No-RT control sample was prepared to detect any potential contamination with genomic DNA. Subsequently, the amplicon sizes were verified by electrophoresis of the PCR products through 4% acrylamide gel.

The primer of the *L. decemlineata* α-amylase gene (LdAmy) was designed using Primer-BLAST (http://www.ncbi.nlm.nih.gov/tools/primer-blast) after a search of the gene sequence (Acc. LOC111504815) at NCBI (NATIONAL CENTER FOR BIOTECHNOLOGY INFORMATION-NCBI, 2012). Primers were designed from exon-exon junction and had a Tm of over 50°C and little likelihood of secondary structure. Leptinotarsa decemlineata ribosomal protein S18 (LdRP18) was used as the endogenous reference gene, as it was stably expressed at different tissues and development stages [47]. The nucleotide sequences of these primers are shown in Table 1.

Table 1: List of primers used in PCR reactions.

Primer Name	Nucleotide Sequence (5' to 3')	Product Length (bp)
LdAmy	F-CCAAAGGTTTTGCCGGTGTA	179
	R-CACGTAAATCCTGACACCAAC	
LdRP18	F-TAGAATCCTCAAAGCAGGTGGCGA	133
	R-AGCTGGACCAAAGTGTTTCACTGC	

Real-time quantitative PCR (RT-qPCR)

The alpha-amylase gene expression level was investigated using real-time quantitative PCR. The concentration of synthesized cDNA was determined using a Nanodrop array spectrophotometer (Nano Ar 2015, Teifsanje P. P. CO., Tehran, Iran). Real-time PCR was carried out with SYBR Green qPCR Master Mix 2x (YT2551, YTA®, Tehran, Iran) according to the manufacturer's protocol in a final volume of 10µL reaction mixtures by using alpha-amylase gene-specific primers and house-keeping gene ribosomal protein S18 primers in Real-Time PCR system (illumine-Eco®, San Diego, CA, USA). The volume of 0.2µL of each forward and reverse primers, with a concentration of 50nM in the reaction, was added to 5µL SYBR Green qPCR Master Mix, 1µL the first-strand cDNA (15ng/µL), and 3.6µL of DEPC treated water.

To check reproducibility, the qPCR reaction for each sample was performed in technical triplicate and biological duplicate. Negative controls without template (NTC) were included in each experiment. The PCR cycling conditions were denaturing 95°C for 3min, and 40 cycles of PCR amplification step at 95°C for 20sec, 50°C for 40sec, 72°C for 25sec and final step 72°C for 3min. A melting curve analysis was performed immediately following the final PCR cycle to confirm the specific qPCR product for each reaction, in other words, to differentiate between the desired amplicons and any primer-dimers or DNA contaminants.

Melt curves stages were 95°C for 15sec, 60°C for 15sec, and 95°C for 15sec. The raw fluorescence data for all runs were imported into the real-time PCR Eco software to determine the threshold cycle (Ct) value. Relative quantities of gene expression ratio were calculated according to the method of Pfaffl (2001) and using the following formulas;

$$Ratio = \frac{\left(E_{target}\right)^{\Delta Ct_{target}(control-sample)}}{\left(E_{ref}\right)^{\Delta Ct_{ref}(control-sample)}}$$

Where; Ratio is the relative gene expression ratio, E_{target} is the real-time PCR efficiency of target gene transcript, E_{ref} is the real-time PCR efficiency of reference gene transcript, ΔCt_{target} is the Ct deviation of control-sample of the target gene transcript, ΔCt_{ref} is the Ct deviation of control-sample of the reference gene transcript.

The amplification efficiency (E) for all RT-qPCR reactions was calculated using the *LinRegPCR* software [48].

Estimation of protein concentration

The protein concentration of samples was estimated according to the method of Bradford (1976), where bovine serum albumin (BSA) was used as a standard protein.

Statistical analysis

Analyses of Variance (ANOVA) were employed on the data and the means of the three replicates were tested by Tukey's test for significant differences. Differences in gene expression were evaluated by ANOVA followed by the T-test. To calculate the relative expression of each target gene, the Ct values were analyzed using Excel software (Microsoft office). The values were presented as the mean ± SE.

Results and Discussion

The inhibition of *L. decemlineata* fourth instar larval digestive α-amylase by Ag/SiO_2 NPs was analyzed by adding 10µL of six different concentrations; 125, 250, 500, 1000, 2000, and 4000 ppm to amylase reactions and enzyme activity inhibition was recorded. Analysis of variance revealed significant differences by Tukey's test ($F=78.756$; $p = 0.0001$) in the α-amylase activity of the larvae by different concentrations of Ag/SiO_2 NPs. The highest inhibitory effect was recorded 72% at 1000 ppm and the least was 21% at 125 ppm (Figure 1).

To understand the effect of Ag/SiO_2 NPs in vivo, insect feeding trials were conducted. Larvae of the CPB were reared from the first instar on potato leaves coated with 1000 ppm Ag/SiO_2 NPs. After ten days the mortality of insects was recorded and compared to control in which leaves were coated by xH_2O. Analysis of variance revealed significant differences in larval mortality compare to control by T-test ($t = 12.061$; $p = 0.0001$). Where the mortality in the control trial was 8%, in the NPs treatment was recorded 65% (Figure 2). Moreover, the surviving fully grown fourth instar larvae in control and treatment were selected for RNA extraction intended for analysis α-amylase gene expression.

The quality of the isolated RNA samples was assessed by agarose gel electrophoresis (Figure 3). The profile of RNA bands differs significantly from standard gels because the 28S rRNA of most insects

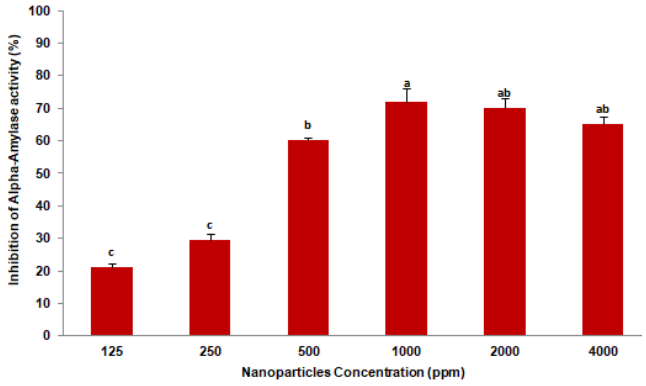

Figure 1: The digestive α-amylase inhibition of *Leptinotarsa decemlineata* fourth instar larvae after the enzyme extract was pre-incubated with Ag/SiO_2 NPs at different concentrations. Each treatment was independently repeated in triplicate. Means followed by the different letters in every data column indicate significant differences between data based on Tukey's test ($p < 0.01$).

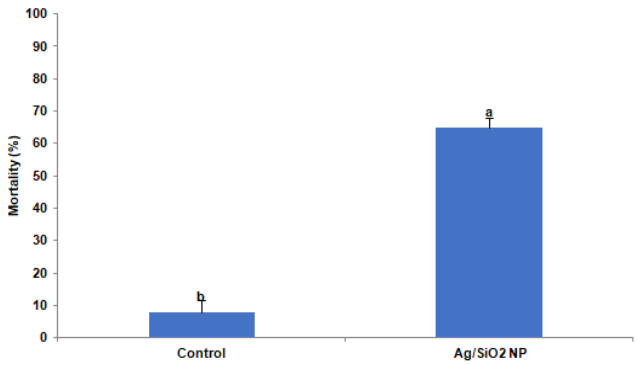

Figure 2: The mortality of *Leptinotarsa decemlineata* larvae after ten days of feeding on potato leaves treated by 1000ppm Ag/SiO_2 NPs. Each treatment was independently repeated in triplicate. Values are presented as the Mean ± SE. Statistical significance between control and treatment was evaluated using the T-test ($p < 0.0001$).

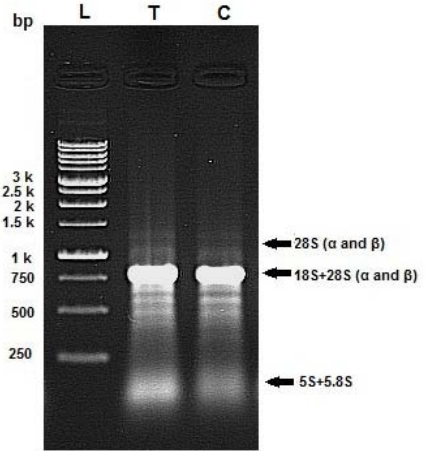

Figure 3: Example of RNA integrity evaluation by agarose gel (1%). Samples of total RNA (2µg) were fractionated on a 1% agarose gel in TBE buffer and stained with ethidium bromide. Lane "T" is related to Ag/SiO_2 NPs treatment and lane "C" is related to control.

contains an endogenous "hidden break" [49,50]. The 28S rRNA of most insects consists of two separate fragments (α and β) that are hydrogen-bonded together. Upon denaturation, disruption of these hydrogen bonds occurs, and both bands migrate closely with 18S rRNA. The 5.8S rRNA is also base-paired to this 28S complex and is likewise released in denaturing conditions [50]. Hence the total RNA extract exhibits a single 18S rRNA band sharply, and others have weak intensity.

After examination of total RNA integrity, RT-PCR was carried out and cDNA was synthesized. It is essential to ensure that the specificity of the primers coding for the reference and template genes is appropriate to be used before real-time qPCR. For this purpose, the cDNA was subjected to PCR amplification assays using the designed primer pairs. The amplification products were resolved on an acrylamide gel (4%) resulting in a unique amplicon of the expected size of 179bp for α-amylase and 133bp for RP18 (Figure 4a). No additional bands or primer-dimer products were detected in any of the amplified DNA samples. On the other hand, polymerase chain reaction products amplified for the gut α-amylase genes of L.

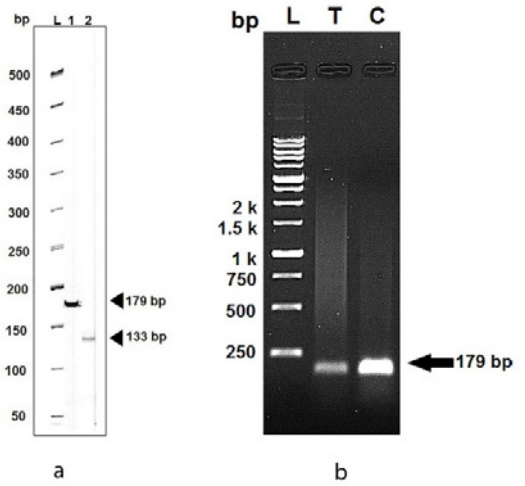

Figure 4: (a) Example of primer specificity analysis using PCR products amplified for the α-amylase gene (Lane 1) and housekeeping gene (Lane 2) of Leptinotarsa decemlineata on acrylamide gel using *DM1100* SMOBIO ExcelBand™ 50bp DNA Ladder. (b) The amplicon of the gut α-amylase genes of larvae grown on treated leaves by Ag/SiO_2 NPs (T) and control (C) On agarose gel (1%) electrophoresis using *DM3100* SMOBIO ExcelBand™ 250bp to 10Kbp DNA Ladder.

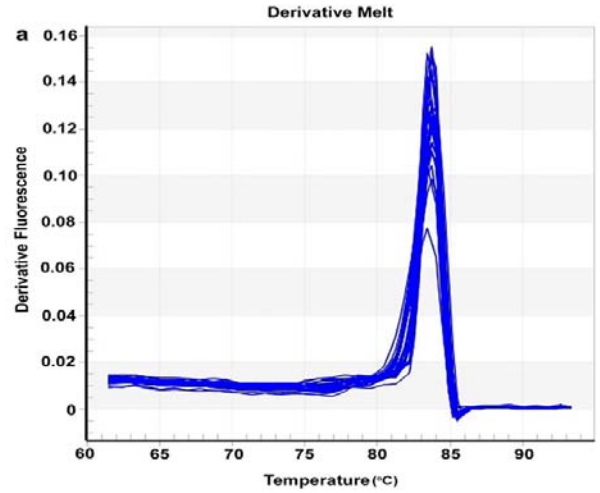

Figure 5: Representative larval gut α-amylase and RP18 of *Leptinotarsa decemlineata* RT-qPCR products melting curves (a) and amplification plot (b). The horizontal line is the threshold.

decemlineata fourth instar larvae grown on treated leaves by Ag/SiO_2 NPs were qualified on agarose gel electrophoresis (Figure 4b). The specificity of the amplification reactions was verified by their single known-sized bands and the intensity of the treatment band was less than control.

After examination of total RNA integrity, RT-PCR was carried out and cDNA was synthesized. It is essential to ensure that the specificity of the primers coding for the reference and template genes is appropriate to be used before real-time qPCR. For this purpose, the cDNA was subjected to PCR amplification assays using the designed primer pairs. The amplification products were resolved on an acrylamide gel (4%) resulting in a unique amplicon of the expected size of 179bp for α-amylase and 133bp for RP18 (Figure 4a). No additional bands or primer-dimer products were detected in any of the amplified DNA samples. On the other hand, polymerase chain reaction products amplified for the gut α-amylase genes of *L. decemlineata* fourth instar larvae grown on treated leaves by Ag/SiO_2 NPs were qualified on agarose gel electrophoresis (Figure 4b). The specificity of the amplification reactions was verified by their single known-sized bands and the intensity of the treatment band was less than control.

The expression profile of the α-amylase gene of larvae on the control (non-treated) and treatment was conducted by quantitative RT-qPCR. For the quantification of results, the threshold cycle (Ct) was determined for each reaction. Ct values for the α-amylase gene were normalized using the obtained Ct values by expression of the internal reference gene ribosomal protein 18 which was reported to be the most stable housekeeping gene in seven developmental stages and three larval tissues of L. decemlineata [47].

The gene expression is calculated by the relative real-time RT-PCR applying the Pfaffl analysis method [51], taking into account the reactions' efficiencies [52]. After calculating ΔCt values and gene expression ratio by the pfaff method, the degree of induction or inhibition of the gene of interest was obtained and calculated as the difference between gene expression of treated sample and control.

PCR efficiency for the amplicon of interest is assumed constant, in the case of the $2^{-\Delta\Delta CT}$ method [53], equal to 2 or are usually calculated from standard curves based on the dilution series of a reference cDNA sample. These approaches can lead to non-specific PCR efficiencies per reaction and they proposed linear regression on the Log (fluorescence) per cycle number data to calculate PCR efficiencies for each sample [48] showed. Therefore, the mean PCR primer efficiency for each reaction was determined by LinRegPCR software.

The melting curve was established after the amplification after the qPCR reaction to verify the presence of nonspecific products or primer-dimers. Melting curve analysis showed that a single peak was formed for the reference gene and the gene of interest and no indication of primer dimerization (Figure 5). The Tm of PCR primers for α-amylase and RP18 ranged from 83 to 84°C.

This section may be divided into subheadings. It should provide a concise and precise description of the experimental results, their interpretation as well as the experimental conclusions that can be drawn.

The calculated expression ratio demonstrated that the gut α-amylase gene of larvae grown on Ag/SiO^2 NPs treated leaves had a significant differentiated expression when compared to the control ($t = 2.885$, $p = 0.0448$). As shown in Figure 6 the significant decrease in expression fold in comparison to the control was observed (0.47-fold). In other words, target gene expression is down-regulated compared to control.

PL (photoluminescence) spectra of the bare nanoparticles and their conjugation with RNA can give useful information about the interaction between surfaces of nanoparticles and RNA. The common phenomenon for the evaluation of bonding between nanoparticles and biomolecules is the investigation of fluorescence resonance

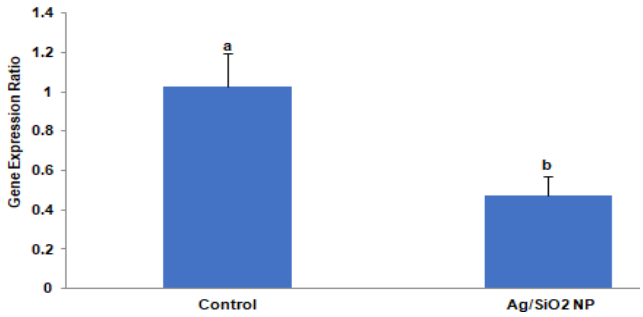

Figure 6: The effects of Ag/SiO_2 NPs on the expression of the α-amylase gene of *Leptinotarsa decemlineata* fourth instar larvae compared to control. The expression level of the target gene was normalized to the expression of ribosomal protein 18. Values are presented as the Mean ± SE. Statistical significance between control and treatment was evaluated using the T-test ($p < 0.05$).

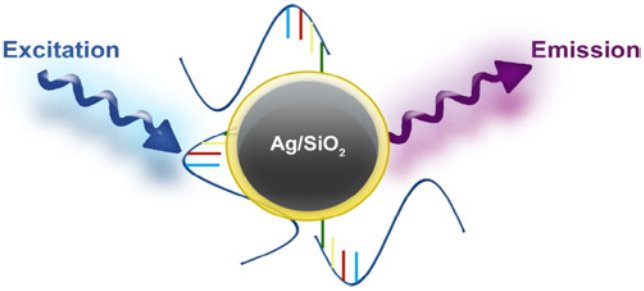

Scheme 1: FRET in RNA-Ag/SiO_2 conjugate.

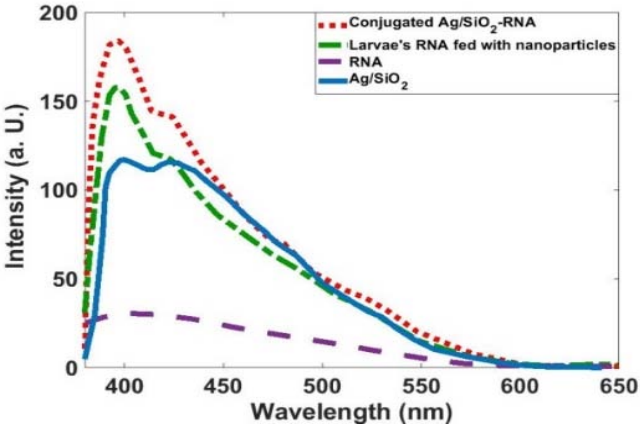

Figure 7: PL spectra of the Ag/SiO_2, RNA, Ag/SiO_2-RNA, and Larvae's RNA fed with Ag/SiO_2 Nanoparticles.

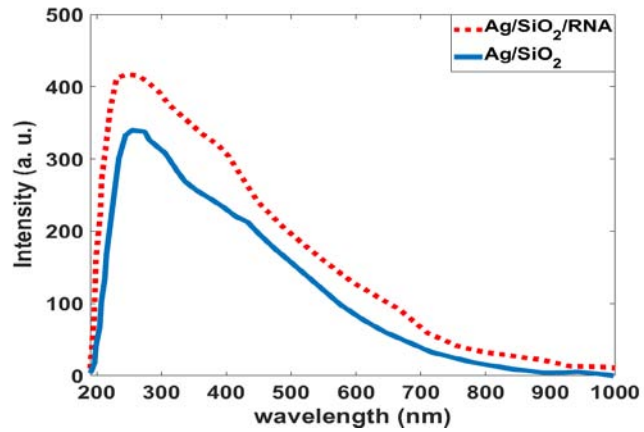

Figure 8: Absorption spectra of the bare and RNA conjugated Ag/SiO_2 nanoparticles.

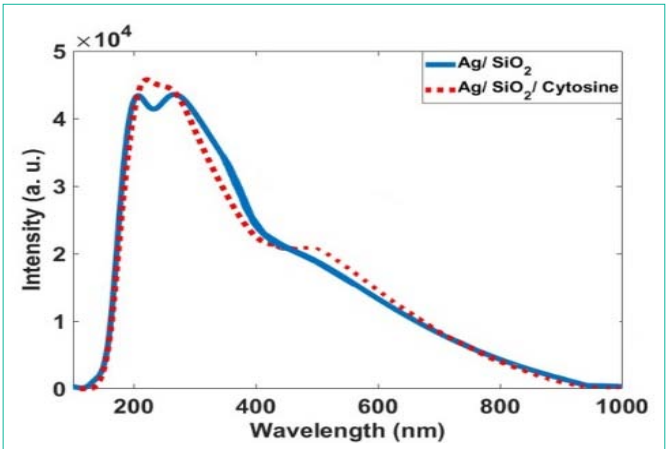

Figure 9: Calculated absorption spectra for the Ag/SiO_2 and Ag/SiO_2-Cytosine.

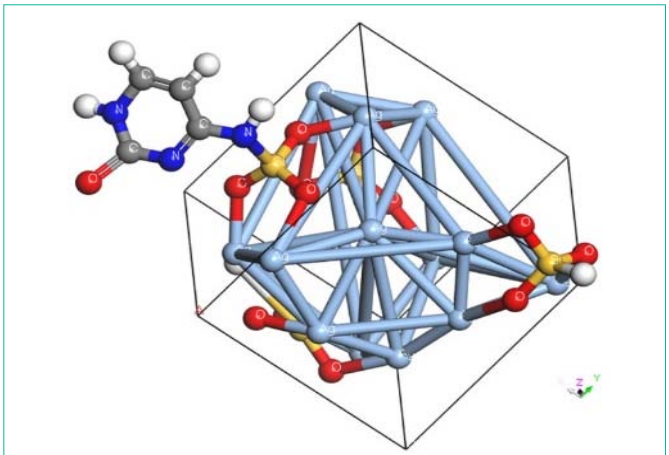

Scheme 2: DFT-calculated optimized cells of Ag/SiO_2 conjugated with Cytosine molecule.

energy transfer (FRET). Spectral evidence of FRET can be explained by the decrease or increase of acceptor emission intensity in two-color FRET systems [28]. Comparative FRET efficiency for the RNA-Ag/SiO_2 is shown in Scheme 1.

Figure 7 shows that the Ag/SiO_2 nanoparticles have emission bands at 405 and 440 nm; this is while alone RNA has almost no emission in the measured wavelengths range. With conjugation of RNA with synthesized nanoparticles intensity of the peak observed at 405nm increases with the fold of 1.5. Increasing the intensity for the peak at 440nm is 1.2 times more than the bare nanoparticle. This figure shows that the Larvae's RNA fed with Ag/SiO_2 nanoparticles is similar to the chemically conjugated RNA-Ag/SiO_2 and only increasing of the intensities of the peaks are less than conjugated RNA-

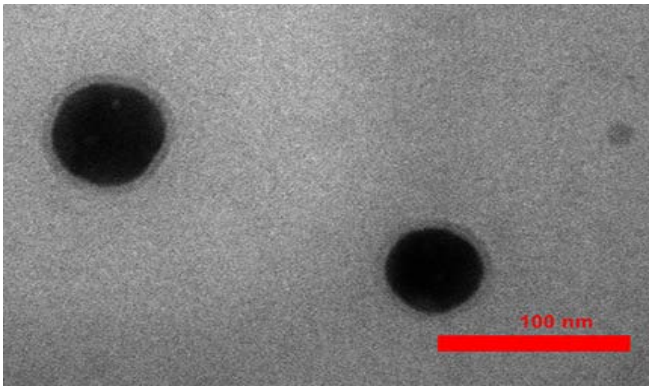

Figure 10: The TEM image of synthesized Ag/SiO_2 nanoparticles.

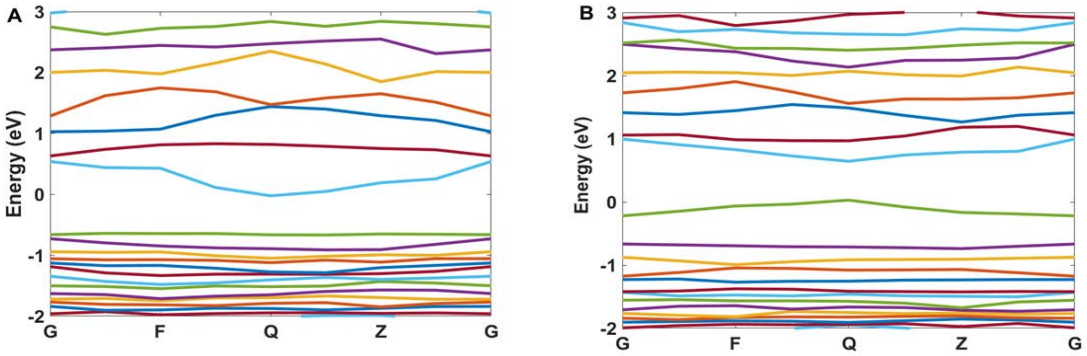

Figure 11: The calculated band structure for A) Ag/SiO_2 and B) Ag/SiO_2/Cytosine.

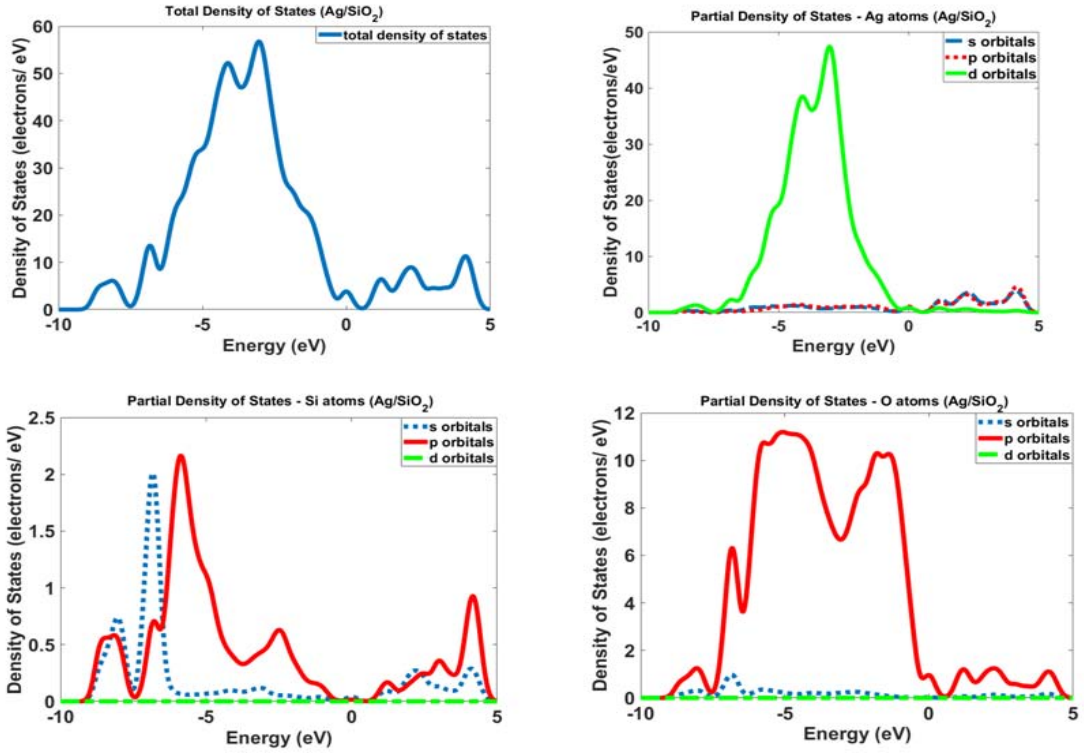

Figure 12: The calculated density of states for Ag/SiO_2 nanoparticles.

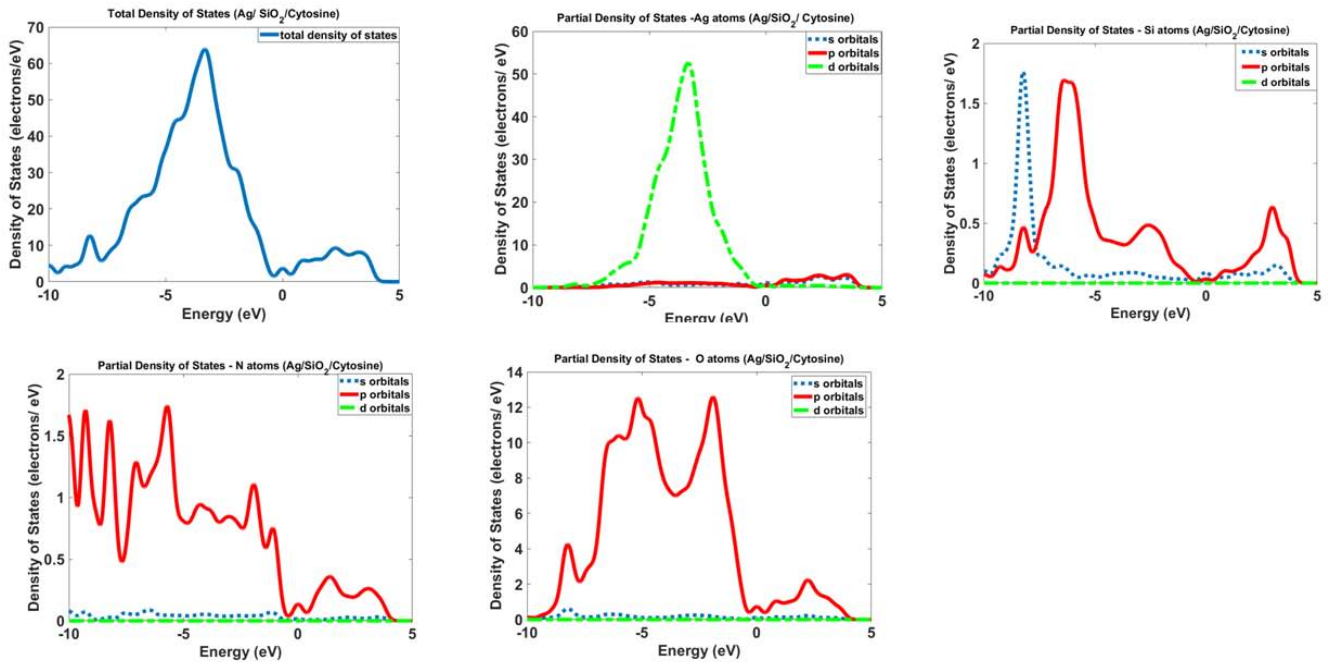

Figure 13: Calculated density of states for Ag/SiO_2 and Ag/SiO_2/Cytosine nanoparticles.

Ag/SiO_2. This means an interaction occurs between the insect's RNA and nanoparticle with feeding the insect with the leaf contaminated with nanoparticles. Absorption spectra of the synthesized Ag/SiO_2 NPs and their conjugation with RNA (Figure 8) show an increase in the intensity and broadening of the spectrum in conjugated NPs. The increase in the intensity is less than emission spectra and the peak of absorption bands is at 280nm.

For more characterization of the occurred phenomenon, we simulated the Ag/SiO_2 and conjugated nanoparticles with DFT calculations. Figure 9 indicates theoretically obtained results for the absorption spectra of the Ag/SiO_2 and Ag/SiO_2-Cytosine. For calculation limitations, we designed the structure with a size of 1.6nm in diameter (Scheme 2). As Figure 9 shows, two bands at 210nm and 290nm are observed for Ag/SiO_2 nanoparticles. With conjugation of the cytosine molecule on the nanoparticle, these two bands overlap together and their intensity of them increases. This increase is more for the first peak at 210nm. As spectra show, there is a good agreement with experimentally obtained absorption spectra although the size of nanoparticles is smaller than real nanoparticles. As the TEM image of the synthesized NPs (Figure 10) shows, the size of particles is about 53nm.

For more explanation of the designed system, the band structure and density of states for Ag/SiO_2 and its conjugation with Ag/SiO_2/Cytosine are calculated. As Figure 11A and 11B shows, some differences occur in the band structure of nanoparticles with the conjugation of cytosine. The important difference is a change in the energy of the band at -0.63eV which converts to 0eV with the conjugation of Cytosine. Also, the band at 0eV converts to 0.5eV for the conjugated system. This means that there is a bandgap for Ag/SiO_2 particle and it is 0.63eV. This gap is 0.5eV for the conjugated system and with attaching cytosine on the surface of the nanoparticle band gap 0.13eV decreases.

Figure 12 and 13 show the calculated density of states for Ag/SiO_2 and Ag/SiO_2/Cytosine nanoparticles. For obtaining more knowledge about optical properties; we investigate electronic transitions in the structures. There are electronic transitions at 210nm (5.9eV) and 290nm (4.27eV). As Figure 11 indicates the probability of these electronic transitions from d orbitals of Ag atoms to the p and s orbitals of Ag atoms is high; however, the contribution of s and p orbitals of Si and O atoms cannot be ignored. In the case of Ag/SiO_2/Cytosine, the probability of electronic transitions from the same orbitals (d orbitals of Ag atoms to s and p orbitals of Ag atoms) is high; however, the density of electrons on d orbitals and p orbitals of O atoms is higher than nanoparticles without Cytosine (Ag/SiO_2) and this causes the higher intensity of electronic transitions in conjugated nanoparticles.

References

1. Agrawal S and Rathore P. Nanotechnology pros and cons to agriculture: a review. Int. J. Curr. Microbiol. Appl. Sci. 2014; 3: 43-55.
2. Kitherian S. Nano and Bio-nanoparticles for insect control. Res. J. Nanosci. Nanotech. 2017; 7: 1-9.
3. Huang B, Chen F and Shen Y. Advances in targeted pesticides with the environmentally responsive controlled release by nanotechnology. Nanomater. 2018; 8: 102.
4. Benelli G. Mode of action of nanoparticles against insects. Envir. Sci. Pollut. Res. 2018; 25: 12329-12341.
5. Clausen CA, Kartal SN, Arango RA and Green F. The role of particle size of particulate nano-zinc oxide wood preservatives on termite mortality and leach resistance. Nanoscale Res. Lett. 2011; 6: 427.
6. Khooshe-Bast Z, Sahebzadeh N, Ghaffari-Moghaddam M and Mirshekar A. Insecticidal effects of zinc oxide nanoparticles and *Beauveria bassiana* TS11 on *Trialeurodes vaporariorum* (Westwood, 1856) (Hemiptera: Aleyrodidae). Acta Agric. Slov. 2016; 107: 299-309.

7. Mommaerts V, Jodko K, Thomassen LC, Martens JA, Kirsch-Volders M and Smagghe G. Assessment of side-effects by Ludox TMA silica nanoparticles following a dietary exposure on the bumblebee *Bombus terrestris*. Nanotoxicology. 2012; 6: 554-561.

8. Panacek A, Prucek R, Safarova D, Dittrich M, Richtrova J, Benickova K, et al. Acute and chronic toxicity effects of silver nanoparticles (NPs) on *Drosophila melanogaster*. Environ. Sci. Technol. 2011; 45: 4974-4979.

9. Kalimuthu K, Panneerselvam C, Chou C, Tseng LC, Murugan K, Tsai KH, et al. Control of dengue and Zika virus vector Aedes aegypti using the predatory copepod *Megacyclops formosanus*: synergy with *Hedychium coronarium*-synthesized silver nanoparticles and related histological changes in targeted mosquitoes. Process Saf. Environ. 2017; 109: 82-96.

10. Bharani RA and Namasivayam SKR. Biogenic silver nanoparticles mediated stress on developmental period and gut physiology of major lepidopteran pest *Spodoptera litura* (Fab.) (Lepidoptera: Noctuidae)-An eco-friendly approach of insect pest control. J. Environ. Chem. Eng. 2017; 5: 453-467.

11. Yasur J and Rani PU. Lepidopteran insect susceptibility to silver nanoparticles and measurement of changes in their growth, development and physiology. Chemosphere. 2015; 124: 92-102.

12. Raj A, Shah P and Agrawal N. Dose-dependent effect of silver nanoparticles (AgNPs) on fertility and survival of Drosophila: An *in-vivo* study. Plos One. 2017; 12: e0178051.

13. Fouad H, Hongjie L, Hosni D, Wei J, Abbas G, Ga'al H, et al. Controlling *Aedes albopictus* and *Culex pipiens* pallens using silver nanoparticles synthesized from aqueous extract of *Cassia fistula* fruit pulp and its mode of action. Artif. Cell, Nanomed. B. 2018; 46: 558-567.

14. Ga'al H, Fouad H, Tian J, Hu Y, Abbas G and Mo J. Synthesis, characterization and efficacy of silver nanoparticles against *Aedes albopictus* larvae and pupae. Pestic. Biochem. Physiol. 2018; 144: 49-56.

15. Rouhani M, Samih MA, Kalantari S. Insecticide effect of silver and zinc nanoparticles against *Aphis nerii* boyer de fonscolombe (Hemiptera: Aphididae). Chil. J. Agr. Res. 2012; 72: 590-594.

16. Sayed AM, Kim S and Behle RW. Characterization of silver nanoparticles synthesized by *Bacillus thuringiensis* as a nanobiopesticide for insect pest control. Biocontrol Sci. Technol. 2017; 27: 1308-1326.

17. Sundararajan B and Kumari BR. Novel synthesis of gold nanoparticles using *Artemisia vulgaris* L. leaf extract and their efficacy of larvicidal activity against dengue fever vector *Aedes aegypti* L. J. Trace Elem. in Med. Biol. 2017; 43: 187-196.

18. Tunçsoy BS. Toxicity of nanoparticles on insects: A Review. Adana Science and Technology University J. Sci. 2018; 1: 49-61.

19. Nair PMG, Park SY, Lee SW and Choi J. Differential expression of ribosomal protein gene, gonadotrophin releasing hormone gene and Balbiani ring protein gene in silver nanoparticles exposed *Chironomus riparius*. Aquat. Toxicol. 2011; 101: 31-37.

20. Nair PMG and Choi J. Identification, characterization and expression profiles of *Chironomus riparius* glutathione S-transferase (GST) genes in response to cadmium and silver nanoparticles exposure. Aquat. Toxicol. 2011; 101: 550-560.

21. Nair PMG, Park SY and Choi J. Evaluation of the effect of silver nanoparticles and silver ions using stress responsive gene expression in *Chironomus riparius*. Chemosphere. 2013; 92: 592-599.

22. Demir E, Vales G, Kaya B, Creus A and Marcos R. Genotoxic analysis of silver nanoparticles in Drosophila. Nanotoxicology. 2011; 5: 417-424.

23. Vales G, Demir E, Kaya B, Creus A and Marcos R. Genotoxicity of cobalt nanoparticles and ions in Drosophila. Nanotoxicology. 2013; 7: 462-468.

24. Ávalos A, Haza AI, Drosopoulou E, Mavragani-Tsipidou P and Morales P. *In vivo* genotoxicity assessment of silver nanoparticles of different sizes by the Somatic Mutation and Recombination Test (SMART) on Drosophila. Food Chem. Toxicol. 2015; 85: 114-119.

25. Carmona ER, García-Rodríguez A and Marcos R. Genotoxicity of copper and nickel nanoparticles in somatic cells of *Drosophila melanogaster*. J. Toxicol. 2018; 7278036.

26. Chandramohan B, Murugan K, Panneerselvam C, Madhiyazhagan P, Chandrasekar R, Dinesh D, et al. Characterization and mosquitocidal potential of neem cake-synthesized silver nanoparticles: genotoxicity and impact on predation efficiency of mosquito natural enemies. Parasitol. Res. 2016; 115: 1015-1025.

27. Li F, Gu Z, Wang B, Xie Y, Ma L, Xu K, et al. Effects of the biosynthesis and signaling pathway of ecdysterone on silkworm (*Bombyx mori*) following exposure to titanium dioxide nanoparticles. Journal of Chemical Ecology. 2014; 40: 913-922.

28. Förster T. Zwischenmolekulare Energieumwandlung und Fluoreszenz. Ann. Physics. 1948; 2: 55-75.

29. Förster T. Energy migration and fluorescence. J. Biomed. Optics. 2012; 17: 011002, 1-10. Translation from Naturwissenschaften. 1946; 33: 166-175.

30. Stryer L. Fluorescence Energy Transfer as a Spectroscopic Ruler. Ann. Rev. Biochem. 1978; 47: 819-846.

31. Jovin TM, Wieb van der Meer B, Hildebrandt N, Sapsford KE, Pons T, Campbell RE, et al. Outlook on FRET: The Future of Resonance Energy Transfer, in FRET - Förster Resonance Energy Transfer: From Theory to Applications (eds I. Medintz and N. Hildebrandt), Wiley-VCH Verlag GmbH & Co. KGaA, Weinheim, Germany. 2013.

32. Lakowicz JR. Principles of Fluorescence Spectroscopy, 3rd ed. Springer, New York. 2006.

33. Dolatyari Rostami, Torabi Klein. Fluorescence Resonance Energy Transfer between an Anti-EGFR Antibody and Bi_2Se_3/SiO_2, ZnS/SiO_2, and $ZnSe/SiO_2$ Nanomaterials for Biosensor Purposes. Z. anorg. Allg. Chem. 2017; 643: 1564-1571.

34. Mathur D, Medintz IL. Analyzing DNA Nanotechnology: A Call to Arms for the Analytical Chemistry Community. Anal. Chem. 2017; 89: 2646-2663.

35. Algar WR, Khachatrian A, Melinger J, AL Huston, M Stewart H, Susumu K, et al. Concurrent Modulation of Quantum Dot Photoluminescence Using a Combination of Charge Transfer and Förster Resonance Energy Transfer: Competitive Quenching and Multiplexed Biosensing Modality. J. Am. Chem. Soc. 2017; 139: 363-372.

36. Dennis AM, Delehanty JB, Medintz IL. Emerging Physicochemical Phenomena along with New Opportunities at the Biomolecular-Nanoparticle Interface. Chem. Phys. Lett. 2016; 7: 2139-2150.

37. Wegner KD, Hildebrandt N. Quantum dots: bright and versatile *in vitro* and *in vivo* fluorescence imaging biosensors. Chem. Soc. Rev. 2015; 44: 4792-4834.

38. Breger J, Delehanty JB, Medintz IL. Continuing progress toward controlled intracellular delivery of semiconductor quantum dots. WIREs Nanomed Nanobiotechnol. 2015; 7: 131-151.

39. Algar WR, Kim H, Medintz IL, Hildebrandt N. Emerging non-traditional Förster resonance energy transfer configurations with semiconductor quantum dots: Investigations and applications. Coord. Chem. Rev. 2014; 263-264: 65-85.

40. Torabi P, Dolatyari M, Rostami G, Oghli AS, Amini P, Rostami A. Nanoparticles-Based Fluorescence Resonance Energy Transfer for Detection of Biotin. J. Colloid Sci. Biotechnol. 2014; 3: 227-231.

41. Clark SJ, Segall MD, Pickard CJ, Hasnip PJ, Probert MJ, Refson K, et al. Materials Studio, CASTEP, version 5.0, San Diego, CA: Accelrys. 2009.

42. Hamann DR, Schlüter M and Chiang C. Norm-Conserving Pseudopotentials. Phys. Rev. Lett. 1979; 43: 1494-1497.

43. Monkhorst HJ and Pack JD. Special points for Brillouin-zone integrations. Phys. Rev. B. 1976; 13: 5188-5192.

44. Cohen RE, Gülseren O and Hemley RJ. Accuracy of equation-of-state formulations. Am. Mineral. 2000; 85: 338-344.

45. Bernfeld P. Amylases, α and β. Method Enzyme. 1955; 1: 149-158.

46. Ashouri S, Farshbaf Pourabad R, Bandani A and Dastranj M. Inhibitory effects of barley and wheat seed protein on digestive α-amylase and general protease activity of *Leptinotarsa decemlineata* Say (Coleoptera: Chrysomelidae). Turk. J. Entomol. 2015; 39: 321-332.

47. Shi XQ, Guo WC, Wan PJ, Zhou LT, Ren XL, Ahmat T, et al. Validation of reference genes for expression analysis by quantitative real-time PCR in *Leptinotarsa decemlineata* (Say). BMC Res. Not. 2013; 6: 93.

48. Ramakers C, Ruijter JM, Deprez RHL and Moorman AF. Assumption-free analysis of quantitative real-time polymerase chain reaction (PCR) data. Neurosci. 2003; 339: 62-66.

49. Fujiwara H and Ishikawa H. Molecular mechanism of introduction of the hidden break into the 28S. Nucleic Acids Res. 1986; 14: 6393-6401.

50. Winnebeck EC, Millar CD and Warman GR. Why does insect RNA look degraded? J. Insect Scie. 2010; 10: 159.

51. Pfaffl MW. A new mathematical model for relative quantification in real-time RT-PCR. Nucleic Acids Res. 2001; 29: e45-e45.

52. Chini V, Foka A, Dimitracopoulos G and Spiliopoulou I. Absolute, and relative real-time PCR in the quantification of tst gene expression among methicillin-resistant *Staphylococcus aureus:* evaluation by two mathematical models. Lett. Appl. Microbiol. 2007; 45: 479-484.

53. Livak KJ and Schmittgen TD. Analysis of relative gene expression data using real-time quantitative PCR and the $2^{-\Delta\Delta CT}$ method. Method. 2001; 25: 402-408.